AIAA AVIATION Forum
June 27-July 1, 2022, Chicago, IL & Virtual
AIAA AVIATION 2022 Forum

10.2514/6.2022-4034

Natural Laminar Flow Airfoil Design via Adjoint-Based Transition Onset Delay

Reza Djeddi,* and Kivanc Ekici†
The University of Tennessee, Knoxville, Tennessee 37996

This work is focused on the aerodynamic shape optimization (ASO) of airfoils with the aim of attaining natural laminar flow (NLF) designs. The two-equation Amplification Factor Transport (AFT) model is utilized for an accurate prediction of the transitional boundary layer flows. The NLF designs are achieved by utilizing two different objective functions. In the first approach, the conventional drag minimization problem is solved with a target lift coefficient. In addition, a second approach is proposed in this work that directly aims at delaying the transition onset on both the pressure and suction sides, thus expanding the natural laminar flow region around the airfoil. It is shown that by utilizing a sigmoid fitting of the turbulence index profile, the transition onset locations can be accurately predicted in a differentiable and smooth fashion, which is essential to the adjoint-based sensitivity analysis of the RANS solver. The efficacy of the proposed technique for NLF design has been tested for NACA 0012 and RAE 2822 airfoils at moderate lift coefficients. Results have shown that a significantly lower drag count can be achieved by delaying the transition onset locations compared to the case where only a drag minimization is sought. Additionally, the transition onset locations on both sides of the airfoil are delayed using our proposed technique which results in a significant expansion of the natural laminar flow region.

Nomenclature

C_f	skin friction coefficient
C_D, C_L	total drag and lift coefficients
$C_{D,f}, C_{D,p}$	friction (viscous) and pressure drag coefficients
$C_{L,f}, C_{L,p}$	friction (viscous) and pressure lift coefficients
c	chord length
d	distance to nearest wall point
E	total energy per unit mass
H_L	local boundary-layer shape factor
h	specific enthalpy
I	objective function
i_t	turbulence index (SA model)
M_∞	free-stream Mach number
$\vec{n}$	outward unit normal vector
$\tilde{n}$	modified amplification factor (AFT model)
p	pressure
Pr	Prandtl number
Re	Reynolds number
S	magnitude of strain rate tensor
$\tilde{S}$	limited or clipped magnitude of strain rate tensor
t	time

*Research Assistant Professor and Lecturer, Department of Mechanical, Aerospace and Biomedical Engineering, Professional Member AIAA.
†Professor, Department of Mechanical, Aerospace and Biomedical Engineering, Senior Member AIAA.

u, v	Cartesian velocity components
x, y	Cartesian spacial components
$\mathbf{x}$	vector of design variables (closure coefficients)
y^+	non-dimensional distance from the first cell to the wall
α	angle of attack
γ , $\tilde{\gamma}$	original and modified intermittency
μ	dynamic viscosity
ν	kinematic viscosity (i.e. viscous diffusivity)
$\tilde{\nu}$	modified eddy viscosity (SA model)
ρ	density
τ	shear stress
σ , σ_n , σ_γ	turbulent Prandtl number (SA model) and its variants in the AFT model
χ	eddy viscosity ratio (SA model)
Ω	vorticity magnitude

I. Introduction

The increasing climate change concerns in the modern day have pushed engineers and designers to develop novel aircraft and aerial vehicles that are environmentally responsible.[1] Therefore, increasing the fuel efficiency and reducing the aerodynamic drag have become the key goals in the commercial aviation industry. One of the main ways for achieving a lower drag is to keep the boundary layer flow laminar which has proven to provide an approximately tenfold decrease in the friction drag than a typical turbulent boundary layer.[2] Considering that friction drag accounts for almost 50% of the total aircraft drag during cruise, delaying the laminar to turbulent transition in the boundary layer would be instrumental to achieving fuel efficient aircraft designs.[3] The natural laminar flow (NLF) technology has proven to be a crucial factor in achieving higher fuel efficiency. Recent studies have shown that NLF technology coupled with flow separation control methodologies can lead to more than 15% reduction of the total drag for typical jetliners at cruise conditions.[4,5] Hence, the NLF technology, that was once primarily used for experimental and conceptual designs, is now more than ever relevant in the design of modern commercial aircraft, business jets, and unmanned aerial vehicles (UAV). This resurgence of the NLF technology in aircraft design can be associated with the recent advances in high-fidelity transition modeling and predictions. Furthermore, the accurate prediction of laminar-to-turbulent transition phenomenon has also proven to be instrumental beyond the extent of NLF technology in everyday computational fluid dynamics (CFD) simulations. In recent years, CFD simulations have shown significant regions of laminar flow over the main wings of typical jetliners that were not necessarily designed with the NLF technologies in mind.[5–8] In fact, accurate prediction of the transition onset directly impacts the boundary layer development, flow separation, friction drag count, and maximum lift coefficient, all of which significantly influence the overall design and performance of the aerodynamic body. While it is generally common for Reynolds-Averaged Navier-Stokes (RANS) simulations to be run in a fully-turbulent mode, ignoring transition prediction in CFD analyses involving flows dominated by laminar regime can significantly reduce the accuracy and reliability of these studies.[9]

With the advances in computational tools and high performance computing resources, several different techniques for predicting the laminar-to-turbulent transition have been developed in recent years that are incorporated into existing RANS solvers.[1,10–19] Arnal et al.[20] and Medida[21] provide extensive reviews of different transition modeling techniques as well as the advantages and disadvantages of each method. In general, there are two classes of transition modeling techniques: (1) those based on a stability analysis and a critical amplification criterion (i.e. the e^N method), and (2) those based on empirical correlations of transition onset. In the former approach, linear stability theory is used to approximate the growth of disturbances in the boundary layer and based on a critical value of amplification ratio, transition onset location is predicted (see Refs.[22,23]). Transition onset functions, on the other hand, are based on correlations determined from experimental data and offer relatively accurate predictions within their calibration database.[24–26] While most of these empirically-based transition models use integral boundary layer properties to define transition onset, Langtry and Menter[12] have introduced the $\gamma - \overline{\mathrm{Re}_{\theta t}}$ model that uses correlations based on local flow properties. Although this model was originally introduced for the k-ω SST turbulence model,[27] it has since been tailored[28] to work with the Spalart-Allmaras[29] turbulence model. More recently, a zero-equation

transition model has been proposed by Bas and Cakmakcioglu[30] that offers relatively accurate predictions of transition onset, separation and reattachement zones without the need to solve an additional transport equation. This correlation-based algebraic transition model uses an intermittency distribution function based on the local information and can handle high free-stream turbulence intensities. Another important and interesting feature of this transition model is that there are only two calibration parameters involved in the transition onset function which can be optimized for different applications. More recently, using the e^N empirically-based correlation method[31,32] of linear stability analysis, Coder and Maughmer[33] formulated the Amplification Factor Transport transition model (AFT2014), which is coupled to the Spalart-Allmaras model by the transported envelope amplification factor. Studied herein, is the more recent and robust version of the AFT transition model (AFT2019)[9] which solves a second transport equation for the intermittency function describing the switch from the laminar regime to the turbulent regime. Compared to the popular four-equation k-ω-γ-$\mathrm{Re}_{\theta t}$ SST turbulence-transition model developed by Langtry and Menter[34] (which favors high free-stream turbulent intensity; suitable for turbomachinery applications), the less expensive three-equation AFT2019 and Spalart-Allmaras model is capable of modeling a broad class of external flows subject to natural transition. As a result, the SA-AFT2019 turbulence and transition models are used in this work for the purpose of NLF design.

In order to design aerial structures based on the NLF technology, it is necessary to develop an aerodynamic shape optimization (ASO) tool based on high-fidelity RANS simulations that accurately predict the laminar to turbulent transition. In fact, the inclusion of transition models in ASO simulations can enable the exploitation of laminar flow for drag minimization. On the other hand, the gradient-based optimization techniques are widely utilized in ASO studies due to their deterministic search of the design space that can reach an "optimum" in fewer iterations compared to stochastic optimization algorithms.[35] However, gradient-based optimization techniques necessitate a smooth and differentiable path between the design variables (that determine and control the aerodynamic shape) and the objective function. As such, a *smooth* variant of the AFT transition model is used in this work to enable the accurate prediction of transition sensitivities with respect to the aerodynamic design.[36] The other key aspect of the ASO computations is the objective function that is sought to be minimized during the design cycles. In almost all ASO studies focused on the NLF design of an airfoil, the objective function is considered to be the total drag coefficient.[5,24,37,38] Given that the friction drag for a laminar boundary layer is almost 90% lower compared to a turbulent one, minimizing the drag count can potentially result in a transition onset delay that can expand the laminar flow region around the airfoil. It is also worth noting that the friction drag accounts for up to 50% of the total aircraft drag in cruise conditions.[37,39,40]

The main objective of this work is to design airfoil and aircraft wings based on the NLF technology with the goal of reduced total drag count while maintaining the desired lift constraint. As mentioned earlier, this can be achieved by solving a drag minimization problem for the aerodynamic structure via a gradient-based optimization tool that utilizes the smooth version of the SA-AFT2019 turbulence and transition models. In this work, however, we also focus on a novel technique for explicitly delaying the transition onset location around the airfoil. As such, the laminar region on the surface of the airfoil will be expanded that can directly reduce the total drag count of the aerodynamic structure. To the best of authors' knowledge, this is the first work reported in the literature to perform a natural laminar flow airfoil design via a direct transition delay for drag reduction using a gradient-based optimization based on the discrete adjoint form of the RANS equations. In the following sections, the governing equations for the SA-AFT2019 models are presented and the numerical considerations for obtaining smooth and differentiable forms of these equations are discussed. Additionally, the procedure for predicting the transition onset location around the airfoil is described and the definition of the optimization problem for ASO is presented. Finally, the results for the NLF design of a symmetric NACA 0012 as well as a super-critical RAE 2822 airfoil at moderate target lift coefficients are presented via two different optimization approaches, i.e., (1) total drag minimization and (2) transition onset delay.

II. Mathematical Formulation

In this section, details of the Spalart-Allmaras (SA) turbulence model and the Amplification Factor Transport (AFT) transition model and their coupling are presented. Additionally, numerical considerations for obtaining the "smooth" and "differentiable" form of the SA-AFT2019 models are presented that can enable the gradient-based aerodynamic shape optimization. Moreover, the procedure used for predicting the

transition onset location in a differentiable fashion is described that enables our objective function for NLF design via transition onset delay.

A. Turbulence and Transition Modeling Equations

1. Amplification Factor Transport (AFT) Transition Model

The basis for the AFT transition model is the solution of a surrogate variable, $\tilde{n}$, called the modified amplification factor, which characterizes the envelope of linearly amplified instabilities throughout the boundary layer. The main advantage of the AFT model that sets it apart from other widely used transition models is that it is built on the premise that integral boundary layer (IBL) quantities, such as shape factor, are estimated using local surrogates. This estimation process relies on the carefully guided calibration of the AFT model closure coefficients based on the fundamental boundary-layer theory. Originally developed by Coder and Maughmer,[41] the AFT model focuses on solving a transport equation for the approximate envelope amplification factor such that

$$\frac{\partial \rho \tilde{n}}{\partial t} + \underbrace{\frac{\partial \rho u_j \tilde{n}}{\partial x_j}}_{\text{convective flux}} - \underbrace{\frac{\partial}{\partial x_j}\left[\sigma_n \left(\mu + \mu_t\right) \frac{\partial \tilde{n}}{\partial x_j}\right]}_{\text{diffusive flux}} = \underbrace{\rho \Omega F_{\text{crit}} F_{\text{growth}} \frac{d\tilde{n}}{d\text{Re}_\theta}}_{\text{source term}} \tag{1}$$

The boundary-layer methods rely on the availability of the integral momentum thickness as well as the integral shape factor to determine the boundary-layer profile.[1] However, the AFT model focuses on "estimating" the integral properties using a *local shape factor*. This local shape factor that was originally proposed in the AFT2017a model[42] is defined as

$$H_L = \frac{d^2}{\mu}\left[\nabla\left(\rho \vec{u} \cdot \nabla d\right) \cdot \nabla d\right] \tag{2}$$

where d is the shortest distance from wall and the gradient of the wall distance in Eq. (2) is a reflection of the wall-normal derivative of the wall-normal momentum as a Galilean-invariant indicator of streamwise velocity gradient. Additionally, the gradient factor described in the definition of the H_L is an indicator of the free-stream pressure gradient. This local shape factor is then mapped on the real shape factor, H_{12}, with details of the model and its source term provided in an earlier work.[36] Unlike the earlier versions of the AFT model, i.e., AFT2014[41] and AFT2017a,[42] where an algebraic intermittency was being used for suppressing turbulence production in the laminar boundary layers, the AFT2017b[43] and later, the AFT2019[9] versions, utilized a transport equation for the modified intermittency, $\tilde{\gamma}$. In this work, we focus on a slightly modified version of the AFT2019 transition model where we solve the transport equation (second governing equation of the AFT model) for the actual intermittency instead. This transport equation is given below

$$\frac{\partial \rho \gamma}{\partial t} + \underbrace{\frac{\partial \rho u_j \gamma}{\partial x_j}}_{\text{convective flux}} - \underbrace{\frac{\partial}{\partial x_j}\left[\left(\mu + \frac{\mu_t}{\sigma_\gamma}\right) \frac{\partial \gamma}{\partial x_j}\right]}_{\text{diffusive flux}} = \underbrace{c_1 \rho S F_{\text{onset}} \left(1 - \gamma\right)}_{\text{production source term}} - \underbrace{c_2 \rho \Omega F_{\text{turb}} \left(c_3 \gamma - 1\right)}_{\text{destruction source term}} \tag{3}$$

where γ is the actual intermittency that with a value of 0 in laminar and 1 in turbulent regimes.[34] This intermittency is a mapping of the "modified" intermittency, $\tilde{\gamma}$, originally used by Coder[9] such that $\tilde{\gamma} = \ln(\gamma)$. It is very important to note that the destruction source term of the intermittency equation is controlled by a F_{turb} function to prevent destruction of intermittency within an already turbulent boundary layer. As such, this allows laminarization in boundary layers with small turbulence Reynolds number while maintaining intermittency in turbulent boundary layers.

It is also important to note that the F_{onset} function in the production source term of the intermittency transport equation is directly related to the solution of the amplification factor equation (Eq. [1]) as well as a critical amplification factor, N_{crit}. In the Langtry-Menter transition model,[34] the value of the free-stream turbulence intensity (FSTI) is used to determine the critical momentum-thickness Reynolds number, $\text{Re}_{\theta,c}$, through special correlations, such as Abu-Ghannam/Shaw criterion,[26] to determine the onset of transition. In the AFT transition model, however, the critical factor, N_{crit}, is directly related to the free-stream turbulence intensity according to the modified[44] Mack's relationship.[45] It is worth noting that a newly calibrated relation similar to the Mack's relationship[45] has been recently developed by the authors to significantly improve the transition prediction accuracy of the AFT model in natural transitional flow regimes.[36]

2. Spalart-Allmaras (SA) Turbulence Model

The AFT model described in this work, is developed with the main intention of being used in conjunction with the one-equation turbulence model of Spalart and Allmaras (SA),[29] defined in its conservative form[46] as

$$\begin{aligned}\frac{\partial \rho\tilde{\nu}}{\partial t} + \underbrace{\frac{\partial \rho u_j \tilde{\nu}}{\partial x_j}}_{\text{convective flux}} - \underbrace{\frac{1}{\sigma}\left[\frac{\partial}{\partial x_j}\left(\rho(\nu+\tilde{\nu})\right)\frac{\partial \tilde{\nu}}{\partial x_j}\right]}_{\text{diffusive flux}} &= \underbrace{\rho c_{b1}\left(1-f_{t2}\right)\tilde{S}\tilde{\nu}}_{\text{production source term}} \\ \underbrace{-\rho\left[c_{w1}f_w - \frac{c_{b1}}{\kappa^2}f_{t2}\right]\left(\frac{\tilde{\nu}}{d}\right)^2}_{\text{destruction source term}} &+ \underbrace{\frac{1}{\sigma}\left[\rho c_{b2}\frac{\partial \tilde{\nu}}{\partial x_i}\frac{\partial \tilde{\nu}}{\partial x_i} - (\nu+\tilde{\nu})\frac{\partial \rho}{\partial x_i}\frac{\partial \tilde{\nu}}{\partial x_i}\right]}_{\text{diffusion source term}}\end{aligned} \tag{4}$$

where $\tilde{S}$ is the "limited" magnitude of the strain rate tensor to avoid having it reach zero or to become negative.[46] In the present work and as recommended by Coder,[9] the *negative* version of the Spalart-Allmaras, i.e., SA-neg, is being used. The SA-neg model is identical to the *standard* model whenever the modified eddy viscosity, $\tilde{\nu}$ is greater than or equal to zero. However, for cases where $\tilde{\nu}$ becomes negative, instead of clipping the turbulence model solution, the source terms are slightly varied details of which are provided in Ref.[29] The SA model described herein, utilizes a "tripping" function, f_{t2}, in the definition of its production and destruction source terms. The goal of the f_{t2} function in the SA model, by design, has been to provide a tripping effect at the transition onset as well as a laminarization effect for small $\tilde{\nu}$ solutions. Therefore, the AFT2019 model exploits this built-in functionality by modifying the f_{t2} term to include the solution of the AFT model intermittency equation such that

$$f_{t2} = c_{t3}\left(1-\gamma\right) \tag{5}$$

where $c_{t3} = 1.2$ according to the SA model.[9,29] Here, the intermittency function, γ, from the AFT transition model is used to directly control the tripping function, f_{t2}, of the SA turbulence model.

3. Boundary Conditions and Numerical Considerations

The transport equations solved for the SA turbulence model as well as the AFT transition model also require proper boundary condition treatments. In general, the SA model uses a Dirichlet boundary condition at both far-field and wall boundaries where $\tilde{\nu}$ is set to zero at viscous walls while being set according to a user-specified eddy viscosity ratio, χ_∞, at inflow and far-field boundaries. For the standard SA model used for "fully-turbulent" test cases, the recommended value of χ_∞ is between 3.0 to 5.0.[29,46] However, in order to avoid saturating the incoming flow in the transitional cases, a smaller value of 0.1 is recommended for χ_∞ when AFT transition model is being utilized. Moreover, the AFT transition model uses a Dirichlet boundary condition for both $\tilde{n}$ and γ at the inflow and far-field with $\tilde{n} = 0.0$ and $\gamma = 1.0$ while using a Neumann condition at outflow and viscous wall boundaries.

Additionally, the switching step function as well as the minimum and maximum functions that are used for the SA-AFT2019 models are non-smooth and discontinuous. In order to make the framework compatible with the gradient-based design optimization, the functions must be modified to make them smooth and differentiable. For this reason, the step function, F_{crit}, that directly controls the entire source term for the amplification factor transport equation is replaced by a modified hyperbolic tangent function.[5,36] Additionally, the minimum and maximum functions must be made smooth as these functions are used substantially in the calculation of the source terms for both of the AFT model equations. Moreover, the minimum and maximum functions are also used in the turbulence model and "smoothing" them would be essentially important for the compatibility of these models with gradient-based design optimization. In this work, the Kreisselmeier-Steinhauser (KS) function[47,48] is used to smooth the minimum and maximum functions.[36]

B. Prediction of the Transition Onset Locations

As mentioned earlier, the main objective of this work is to obtain NLF airfoil designs via aerodynamic shape optimization by directly delaying the transition onset locations on suction and pressure sides of the airfoil.

Therefore, it is necessary to accurately predict the transition onset location in a way that would enable the gradient-based optimization toolbox to attain a differentiable path between the objective function and the design variables. It has been shown in an earlier work by the authors[36] that, using a non-linear least-squares minimization problem, one can fit a sigmoid (hyperbolic tangent) function to the "turbulence index" profile for accurate and efficient prediction of the onset locaton. The turbulence index proposed by Spalart and Allmaras in their seminal work[29] is defined as

$$i_t = \frac{1}{\kappa u_\tau} \frac{\partial \tilde{\nu}}{\partial n} \tag{6}$$

where wall shear velocity, u_τ, is approximated as $u_\tau \approx \sqrt{\nu \Omega}$, and n is the wall-normal direction. The turbulence index described in Eq. (6) will have a value close to zero in laminar regions while switching rapidly to a value close to one in turbulent regions. According to Spalart and Allmaras,[29] the value of i_t can rise slightly above one in the turbulent boundary layer as it approaches separation. As such, for a typical turbulence index profile, the transition onset location is determined based on the location at which the sigmoid function that was fitted to the turbulence index profile reaches a value of 0.5. Authors showed in an earlier work the viability of this approach for predicting the transition onset location on a flat plate for calibration studies.[36] In this work, however, the goal is to optimize airfoil geometries where the laminar-to-turbulent transition occurs on both the pressure and suction sides of the airfoil. As such, the proposed methodology described earlier is extended to predict both onset locations via a similar sigmoid fit. For example, the skin friction and the turbulence index profiles over the NACA 0012 airfoil are shown in Fig. (1) for the case run at Mach 0.2 and Reynolds number of four million with a free-stream turbulence intensity of 0.15%.

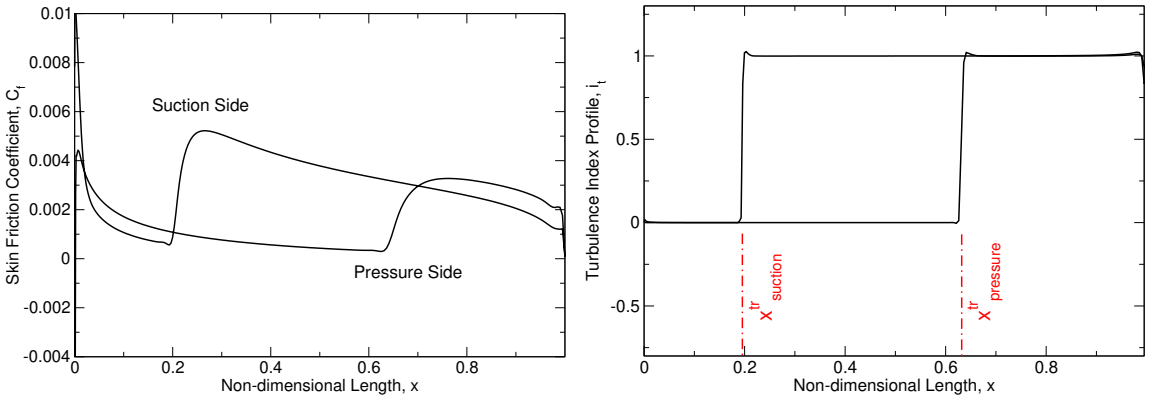

(a) Skin Friction Coefficient

(b) Turbulence Index

Figure 1. Skin friction and turbulence index profiles for the NACA 0012 airfoil at M = 0.2, Re = 4 million, and FSTI = 0.15%.

Here, the angle of attack is calibrated to achieve a target lift coefficient of 0.3 which results in the laminar-to-turbulent transition occuring on both sides of the airfoil. As can be seen in Fig. (1), the boundary layer trips at around 20% chord length on the suction side while the transition onset is located at around 65% chord length on the pressure side of the airfoil. The proposed technique for predicting the transition onset location utilizes two sigmoid functions to fit the turbulence index profiles on both sides of the airfoil. As a result, the two transition onset locations can be accurately predicted in a way that is also differentiable and smooth which is necessary for gradient-based design optimization.

C. Aerodynamic Shape Optimization

As discussed earlier, the goal here is to perform an aerodynamic shape optimization (ASO) of an airfoil with natural laminar flow (NLF) considerations. The objective function for such an optimization problem is typically considered to be the drag coefficient that needs to be minimized. Given that the friction drag is the main contributor to the total drag count for transitional flow cases, the minimization of the drag coefficient

can potentially lead to transition delay and the expansion of the laminar flow region around the airfoil.[5,37] As such, the optimization problem is given as

$$\begin{aligned} \min \quad & C_D \\ \text{w.r.t} \quad & \mathbf{x}, \alpha \\ \text{subject to} \quad & C_L = C_L^* \end{aligned} \tag{7}$$

where $\mathbf{x}$ is the vector of design variables that define and control the geometry and α is the angle of attack. Additionally, C_L^* is the target lift coefficient that must be preserved during the design optimization process. The equality constraint for the target lift coefficient can be easily replaced by an "equivalent" inequality constraint such that

$$\begin{aligned} \min \quad & C_D \\ \text{w.r.t} \quad & \mathbf{x}, \alpha \\ \text{subject to} \quad & |C_L - C_L^*| \leq \epsilon \end{aligned} \tag{8}$$

where ϵ is simply a relaxation threshold for the original equality constraint and is taken to be 0.001 in this work. Ultimately, a penalty function approach is used herein for the inequality-constrained optimization problem such that the following objective is considered for the minimization problem defined in Eq. (7)

$$I = C_D + \gamma_p \, p^+ \left(C_L, C_L^*\right) \tag{9}$$

where p^+ is the penalty function defined as

$$p^+ \left(C_L, C_L^*\right) = \begin{cases} 0 & |C_L - C_L^*| \leq \epsilon \\ \left(C_L - C_L^*\right)^2 & |C_L - C_L^*| > \epsilon \end{cases} \tag{10}$$

where γ_p is the regularization or penalty factor which must be set properly for each constrained optimization problem. Additionally, a two-dimensional Free-Form Deformation (FFD) box[49,50] is used to parameterize the airfoil geometry where the control points of the FFD box are taken to be the design variables, $\mathbf{x}$, shown earlier in the definition of the optimization problem.

In addition to the conventional objective function based on the drag minimization that is given in Eq. (9), we focus on a novel technique for NLF design that seeks to directly delay the transition onset locations on the airfoil. In this approach, the transition onset locations on both the suction and pressure sides of the airfoil are pushed toward a target location in an aerodynamic shape optimization that mimics an inverse design problem. By considering the target locations for the transition onset to be at the trailing edge of the airfoil, it would be possible to achieve an airfoil design with an expanded laminar flow region. Therefore, the objective function for this proposed approach is defined as

$$I = \frac{1}{2}\left(x_{\mathrm{s}}^{\mathrm{tr}} - x_{s,\mathrm{target}}^{\mathrm{tr}}\right)^2 + \frac{\gamma_{\mathrm{tr}}}{2}\left(x_{\mathrm{p}}^{\mathrm{tr}} - x_{p,\mathrm{target}}^{\mathrm{tr}}\right)^2 + \gamma_p \, p^+ \left(C_L, C_L^*\right) \tag{11}$$

where $x_{\mathrm{s}}^{\mathrm{tr}}$ and $x_{\mathrm{p}}^{\mathrm{tr}}$ are the transition onset locations on the suction and pressure sides of the airfoil, respectively. Also, the "target" locations for the transition onset on both sides are set to the trailing edge of the airfoil. Additionally, γ_{tr} is used as a regularization factor to equalize the magnitudes of the two inverse-design objectives used in Eq. (11). Finally, the ASO problems defined herein are solved using discrete adjoint-based optimization within our in-house UNstructured PArallel Compressible Design Optimization Framework (UNPAC-DOF)[51,52] that utilizes our novel Discrete Adjoint with Recursive Technique (DART) framework.[53]

III. Natural-Laminar-Flow Design Optimization Results

In this section, we first present some aerodynamic shape optimization results involving the natural laminar flow design of a symmetric NACA 0012 airfoil at low-speed and low-turbulence flow conditions with a moderate target lift coefficient. Next, the NLF design for a super-critical airfoil at high Mach number and low-turbulence flow conditions will be studied. The NLF design is performed using two different approaches:

(1) the conventional approach by minimizing the total drag coefficient, and (2) the newly proposed technique which directly delays the transition onset locations. As mentioned earlier, we believe this to be the first adjoint-based study reported in the literature that utilizes a direct transition onset delay mechanism for NLF airfoil design.

A. Symmetric NACA 0012 Airfoil

The NACA 0012 airfoil used for the present NLF design is subject to subsonic flow at Mach 0.2 and a Reynolds number of four million. The free-stream turbulence intensity is taken to be 0.15% which is low enough to promote a natural transition of boundary layer on both sides of the airfoil. The target lift coefficient is taken to be $C_L^* = 0.3$ which is maintained via the equivalent inequality constraint as described in the previous section. The penalty factor for the inequality lift-constraint is set to $\gamma_p = 6 \times 10^3$ based on the original drag count of 59.3 and the desired target lift coefficient. For the original design, the angle of attack is calibrated to 2.655 degrees with the drag and lift coefficient breakdowns presented in Table (1).

Table 1. Breakdowns of the lift coefficient and drag counts for the original NACA 0012 airfoil design at Mach 0.2, Re = 4 million, and FSTI = 0.15%.

C_L	$C_{L,p}$	$C_{L,f}$	C_D	$C_{D,p}$	$C_{D,f}$
0.29996	0.30007	-0.00011	59.8402	13.3651	46.4743

As can be seen, the friction drag corresponds to more than 77% of the total drag count for the original design. At the same time, the lift coefficient due to friction only accounts for 0.04% of the total lift produced by the airfoil. As a result, significant reduction in the drag count can be realized by promoting a natural laminar flow design. In order to parameterize the airfoil geometry, a two-dimensional FFD box with 21 control points on each side is used where those points are clustered toward the leading and trailing edges of the airfoil. Furthermore, the control points are fixed at the two ends in order to maintain the incidence flow angle throughout the design cycles. Therefore, with the addition of the angle of attack, a total of 39 design variables are used for the optimization cases presented herein.

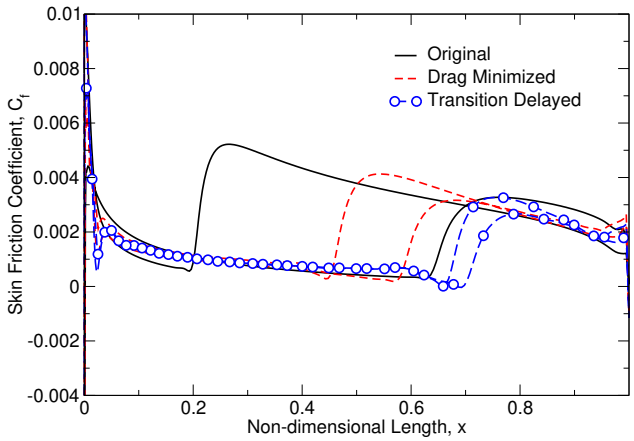

Figure 2. Skin friction coefficient profiles for the NLF design of the NACA 0012 airfoil at Mach 0.2, Re = 4 million, and FSTI of 0.15% (target lift $C_L^* = 0.3$).

As discussed earlier, two different optimizations are considered for the NLF design of the NACA 0012 airfoil. These objective functions are described below:

1. **Objective 1:** drag minimization with the target lift constraint (**"Drag Minimized"**)
2. **Objective 2:** transition onset delay with the target lift constraint (**"Transition Delayed"**)

It is worth noting that in the latter approach, the transition onset locations on both suction and pressure sides can be pushed toward the trailing edge of the airfoil in an effort to achieve a fully expanded natural

laminar flow region. Both optimization problems are solved using a bound-constrained L-BFGS optimizer with the FFD box control points allowed to move ±10%, and the angle of attack varied by ±2.0 degrees.

The results presented here pertain to the skin friction coefficient profiles on the airfoil for the original as well as the two "optimal" designs and are shown in Fig. (2). As can be easily noticed, the laminar region that results in the lower skin friction coefficient is expanded on the suction side for both NLF design cases. However, the transition onset location on the pressure side is shifted slightly toward the leading edge in the first approach that focuses on the drag minimization. This results in the boundary layer tripping sooner on the pressure side which can potentially increase the friction drag coefficient. However, since the transition is delayed on the suction side of the airfoil, the overall drag count will be reduced. The breakdowns of the lift and drag coefficients for the original and optimal designs are presented in Table (2).

Table 2. Breakdowns of the lift coefficient and drag counts for the original and NLF designs of the NACA 0012 airfoil at Mach 0.2, Re = 4 million, and FSTI = 0.15% (target lift $C_L^* = 0.3$).

Design	C_L	$C_{L,p}$	$C_{L,f}$	C_D	$C_{D,p}$	$C_{D,f}$
Original	0.29996	0.30007	-0.00011	59.840	13.365	46.474
Drag Minimized	0.30041	0.30005	-0.00009	48.133	9.5541	38.579
Transition Delayed	0.29960	0.29962	-0.00002	37.644	9.3415	28.303

As can be seen, the total drag count is reduced by almost 20% using the drag minimization approach while a much more significant reduction of 37% has been achieved by directly delaying the transition onset locations. At the same time, the target lift coefficient is maintained within the relaxation threshold used for incorporating the equivalent inequality constraint in the optimization problem. As mentioned earlier, the initial angle of attack for the NACA 0012 airfoil is 2.655 degrees. During the optimization, the angle of attack is reduced to 1.824 and 1.01 degrees for the drag minimization and transition delay approaches, respectively.

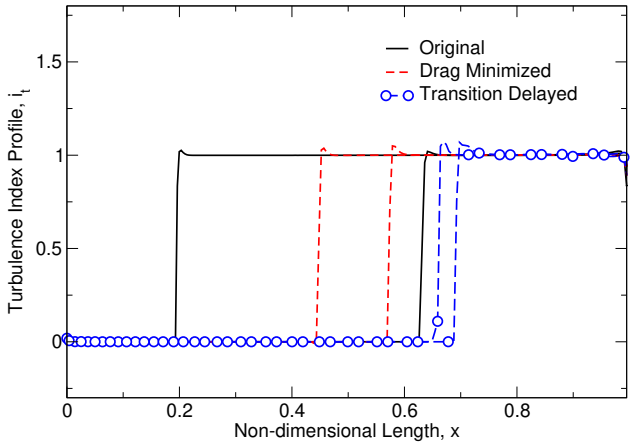

Figure 3. Turbulence index profiles for the NLF design of the NACA 0012 airfoil at Mach 0.2, Re = 4 million, and FSTI of 0.15% (target lift $C_L^* = 0.3$).

Table 3. Non-dimensional transition onset locations on the suction and pressure sides of the original and NLF designs of the NACA 0012 airfoil at Mach 0.2, Re = 4 million, and FSTI = 0.15% (target lift $C_L^* = 0.3$).

Design	x_s^{tr}/c	x_p^{tr}/c
Original	0.195	0.631
Drag Minimized	0.447	0.572
Transition Delayed	0.661	0.691

Next, the turbulence index profiles for the original and the NLF designs are shown in Fig. (3). It can be seen that unlike the drag minimization approach (objective 1), our proposed technique with the transition

delay is capable of pushing both transition onset locations further downstream. Therefore, the laminar flow region is much larger for this NLF design which naturally results in a significantly lower drag count. This can also be seen in Table (3) where the transition onset locations on both sides of the airfoil are presented for the original as well as both NLF designs.

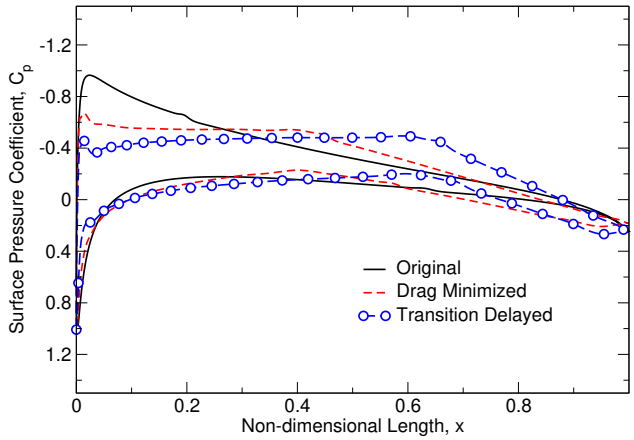

Figure 4. Surface pressure coefficient profiles for the NLF design of the NACA 0012 airfoil at Mach 0.2, Re $= 4$ million, and FSTI of 0.15% (target lift $C_L^* = 0.3$).

The variations of the transition onset locations can be further analyzed and explained by studying the surface pressure profiles. Therefore, the surface pressure coefficients for the original and the two NLF designs are provided in Fig. (4). The boundary layer on the suction side of the airfoil trips very soon at around 20% chord length which means that delaying the onset location on the suction side would have a significant impact on the total drag count of the airfoil. This rapid transition from laminar-to-turbulent boundary layer can be explained by the adverse pressure gradient, $dp/dx > 0$, that covers almost the entire length of the airfoil on the suction side. In the NLF designs, however, a slightly negative pressure gradient is achieved on the suction side which results in the delay of the transition. This favorable pressure gradient is extended longer in the second NLF design with "transition delay" being used as the objective function which explains why the onset location is pushed further downstream.

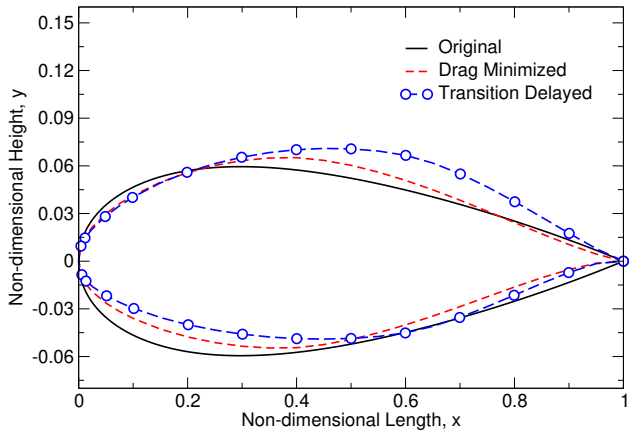

Figure 5. Airfoil geometries for the NLF design of the NACA 0012 airfoil at Mach 0.2, Re $= 4$ million, and FSTI of 0.15% (target lift $C_L^* = 0.3$).

As shown earlier, the transition onset location on the pressure side of the airfoil was pushed slightly upstream in the first NLF design approach, thus compensating to some extent for the extreme delay in transition that was achieved on the suction side of the airfoil. However, in the second NLF design approach, the transition onset on the pressure side is also pushed downstream. This behavior can be further explained by the favorable pressure gradient, $dp/dx < 0$, that is achieved on the lower surface of the airfoil which results in the extension of the laminar flow region and the delay of transition. The original and optimal

shapes of the airfoil are also shown in Fig. (5). It is worth noting that while the cross-sectional area and the minimum thickness parameters were not included as additional constraints in the optimization problem, the airfoil cross-sectional areas for both NLF designs are within ±5% of the original design with less than ±0.5% variations in the airfoil thickness.

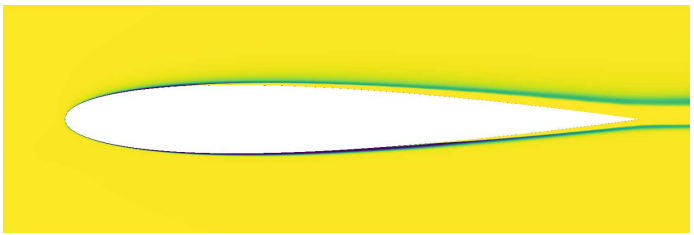

(a) Original

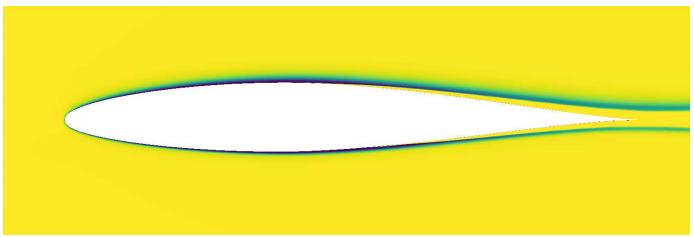

(b) Drag Minimized

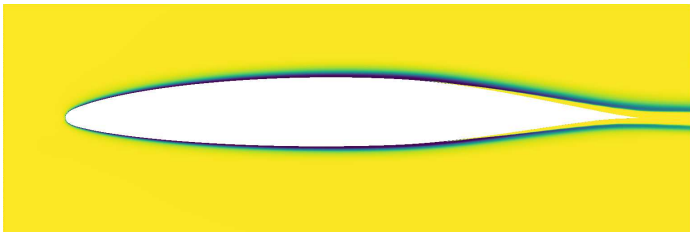

(c) Transition Delayed

Figure 6. Contours of intermittency (SA-AFT2019 model) for the original and the optimal designs of the NACA 0012 airfoil at Mach 0.2, Re = 4 million, and FSTI of 0.15% (target lift $C_L^* = 0.3$). Contour range is from 0 (purple, fully laminar) to 1 (yellow, fully turbulent)

Finally, the contour fields of intermittency solution are shown in Fig. (6) for the original and the optimal designs. As can be seen, the purple region, which corresponds to laminar flow with an intermittency function value of zero, is expanded for both NLF designs. This expansion, however, is more significant for the second approach that aims at delaying the transition onset locations on both sides of the airfoil. As a result, a natural laminar flow is formed for an extended portion of the airfoil, thus resulting in a significant reduction in the drag count.

B. Super Critical RAE 2822 Airfoil

Having presented the design optimization results for the symmetric NACA 0012 airfoil, we now focus our attention to the NLF design of a super critical RAE 2822 airfoil. The NLF design of the RAE 2822 airfoil has been studied previously in the literature where the aerodynamic shape optimization is driven exclusively based on a drag minimization problem. It is important to note that for the super critical RAE 2822 airfoil, studies have focused on minimizing the total drag coefficient, rather than simply the friction drag, given

that the pressure or wave drag components can become significant contributors to the overall aerodynamics and efficiency of the airfoil. As such, Rashad and Zingg[24] used an iterative laminar-to-turbulent transition prediction methodology based on a simplified e^N method. In that work, the NLF design of the RAE 2822 airfoil is performed using single and multi-point optimization approaches based on subsonic and transonic flow conditions at low to moderate lift coefficients, loosely approximating the cruise flight conditions of the Cessna 172R, the Bombardier Dash-8 Q400 turboprop, and the Boeing 737-800 turbofan.[24] Additionally, Halila et al.[5] used a smooth version of the AFT transition model coupled with the SA turbulence model for an adjoint-based design optimization of the RAE 2822 airfoil. It is important to note that Halila et al.[5] performed NLF design for the super critical RAE 2822 airfoil at transonic conditions with a very high lift constraint that results in a strong shock formation as well as shock wave-boundary layer interactions (SWBLI) that can further complicate the NLF design for typical cruise flight conditions. More recently, Shi et al.[37] used a simplified e^N-based transition prediction framework coupled with a database method for flow stability analysis to perform NLF design for the RAE 2822 airfoil. In that work, a multi-point optimization based on total drag minimization is utilized focusing on several design and off-design points during cruise flight and climb conditions for the Cessna 172 SP Skyhawk.[37] In the present work, the NLF design of the super critical RAE 2822 airfoil is considered at a single design point corresponding to the typical cruise conditions of the Cessna 172. The flow conditions are $M = 0.7$ and $\mathrm{Re} = 8 \times 10^6$, where the lift coefficient is constrained to $C_L^* = 0.4$. Additionally, the free-stream turbulence intensity is taken to be 0.15% (corresponding to $\mathrm{N_{crit}} \approx 7.2$ according to the modified[44] Mack's relationship[45]) to once again promote a natural transition of the boundary layer on both sides of the RAE 2822 airfoil. For the original design, the angle of attack is tuned at 0.497 deg to achieve the desired lift coefficient. Additionally, 21 FFD box control points are used on each side of the airfoil for shape parameterization. It is important to note that the FFD control points are clustered toward the leading and trailing edges with the first and last points being fixed to maintain the apparent angle of attack for the airfoil.

Table 4. Breakdowns of the lift coefficient and drag counts for the original RAE 2822 airfoil design at Mach 0.7, Re = 8 million, and FSTI = 0.15%.

C_L	$C_{L,p}$	$C_{L,f}$	C_D	$C_{D,p}$	$C_{D,f}$
0.4003236	0.4003291	-0.000005	52.0035	12.8166	39.1869

The lift and drag (count) coefficient breakdowns for the original design are presented in Table (4). It is apparent that the friction drag dominates the total drag and correspond to more than 75% of the total drag count for the original RAE 2822 airfoil geometry for a moderate lift coefficient of 0.4. This means that by delaying the laminar-to-turbulent transition and expanding the laminar flow region around the airfoil, the friction drag may be reduced offering potentially significant reductions in the total drag count. In addition to the FFD box control points that are used for shape parameterization, the angle of attack is also included as a design variable in order to achieve feasible solutions based on the specified lift constraint.

Table 5. Breakdowns of the lift coefficient and drag counts for the original and NLF designs of the RAE 2822 airfoil at Mach 0.7, Re = 8 million, and FSTI = 0.15% (target lift $C_L^* = 0.4$).

Design	C_L	$C_{L,p}$	$C_{L,f}$	C_D	$C_{D,p}$	$C_{D,f}$
Original	0.400323	0.400329	-0.00001	52.003	12.817	39.187
Drag Minimized	0.400081	0.400083	-0.00002	43.123	10.349	32.773
Transition Delayed	0.399821	0.399824	-0.00003	39.937	10.184	29.753

Similar to the NLF design for the NACA 0012 airfoil, two objective functions are considered for the aerodynamic shape optimization. The first objective is the total drag (conventional approach) while the second objective is defined based on the direct transition delay on both sides of the airfoil (proposed approach in this work). Additionally, both optimizations are carried out using a bound-constrained L-BFGS optimizer where the FFD box control points are allowed to move ±10%. Furthermore, the angle of attack is bounded by ±2.0 degrees. The results presented here pertain to the breakdowns of the lift and drag coefficients for the original and optimal designs which are presented in Table (5). As can be seen, the drag count is reduced for both optimal designs while the "transition delay" approach resulting in a more significant reduction of the

friction drag compared to the standard "drag minimization" case. As a result, similar to the results presented earlier for the design optimization of the NACA 0012 airfoil, the proposed technique based on the direct delay of the transition onset location has resulted in a much better NLF design for the super critical RAE 2822 airfoil. From Table (5), it can be seen that the total drag count is reduced by almost 17.5% using the drag minimization approach while a much more significant reduction of 25% has been achieved by directly delaying the transition onset locations. Additionally, the feasibility condition for the target lift constraint is met for both optimal design cases. It is also important to note that the angle of attacks for the optimal design cases are slightly reduced to 0.378 and 0.386 degrees for the drag minimization and transition delay approaches, respectively.

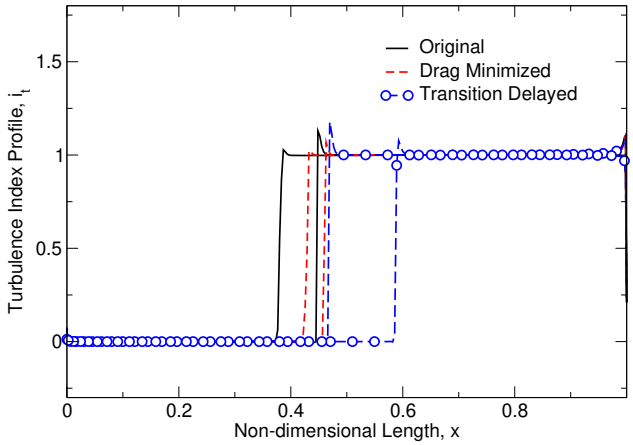

Figure 7. Turbulence index profiles for the NLF design of the RAE 2822 airfoil at Mach 0.7, Re = 8 million, and FSTI of 0.15% (target lift $C_L^* = 0.4$).

The significant reduction in the total drag count is a direct result of a significant delay in the transition onset that is achieved by explicitly pushing the onset locations on both sides of the airfoil toward the trailing edge (target location). This phenomenon can be clearly understood from the turbulence index profiles that are presented in Fig. (7). Both "optimal" cases delay of the laminar-to-turbulent transition. However, the transition delay, especially on the suction side of the RAE 2822 airfoil, is more significant for the "transition delayed" case based on our proposed technique for NLF design.

Table 6. Non-dimensional transition onset locations on the suction and pressure sides of the original and NLF designs of the RAE 2822 airfoil at Mach 0.7, Re = 8 million, and FSTI = 0.15% (target lift $C_L^* = 0.4$).

Design	x_s^{tr}/c	x_p^{tr}/c
Original	0.381	0.448
Drag Minimized	0.428	0.457
Transition Delayed	0.586	0.465

As presented in Table (6), the transition onset location on the suction (top) side of the RAE 2822 airfoil is delayed by 12.3% and 53.8% for the drag minimization and transition delayed approaches, respectively. The significant delay in transition that is achieved using the "transition delay" approach, once again proves the efficacy of the proposed technique for the NLF design. This has resulted in a vast expansion of the laminar regime, especially on the top side, which has resulted in a significantly lower drag count. Additionally, the onset location on the pressure (bottom) side of the airfoil is delayed by only 2-4%. This delay in the laminar-to-turbulent transition, while insignificant, can still contribute to a reduction of the total drag count for the optimal designs studied herein.

Next, the skin friction and surface pressure coefficients are compared for the original and optimal designs and the results are provided in Fig. (8). The skin friction profiles clearly demonstrate a sharp increase in the skin friction coefficient at the transition onset location that results in a sudden increase in the friction drag count. Additionally, the delay in the laminar-to-turbulent transition can be noticed from these C_f profiles. More importantly, it can be easily seen from the surface pressure profiles plotted in Fig. (8(b)) that the

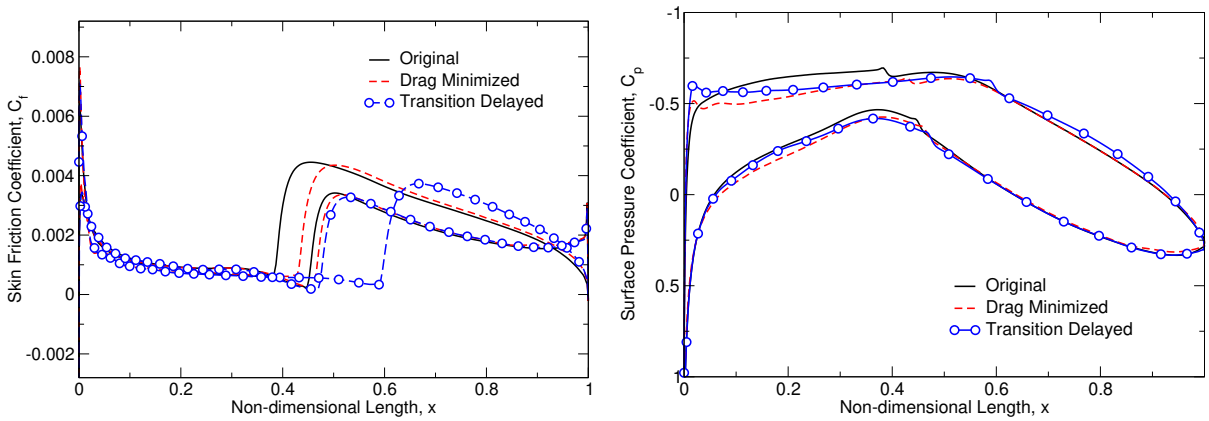

(a) Skin friction, C_f

(b) Surface pressure, C_p

Figure 8. Skin friction and surface pressure coefficients for the NLF design of the RAE 2822 airfoil at Mach 0.7, Re = 8 million, and FSTI of 0.15% (target lift $C_L^* = 0.4$).

optimal designs lead to an extension of the favorable pressure gradient, $dp/dx < 0$, which further accelerates the boundary layer flow. This negative pressure gradient, which was already present in the original design, is extended even longer in the second NLF design with "transition delay." As a result, a delay in transition and, subsequently, an expansion of the laminar flow regime on the top side of the airfoil is achieved.

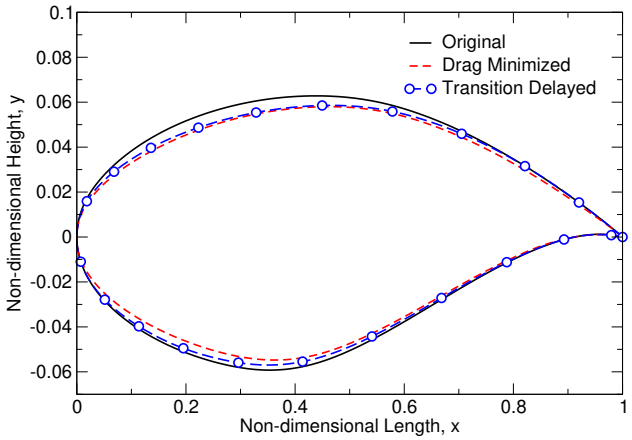

Figure 9. Airfoil geometries for the NLF design of the RAE 2822 airfoil at Mach 0.7, Re = 8 million, and FSTI of 0.15% (target lift $C_L^* = 0.4$).

The original and optimal shapes of the super-critical airfoil are also shown in Fig. (9). It is important to note that the drag minimization approach has resulted in a thinner airfoil that is contracted from top and bottom, thus reducing the curvature and the form drag. In fact, the maximum airfoil thickness is reduced by almost 9% while the airfoil cross-sectional area is also reduced by almost 10%. On the other, the transition delay technique that is proposed in the present work has resulted in a lower-cambered airfoil. Thus, the optimal design has resulted in a flatter suction side with reduced curvature while the bottom side has mostly retained the original shape of the RAE 2822 airfoil. As such, the maximum airfoil thickness is only reduced by 5% whereas the cross-sectional area is shrunk by 7.5%. It must be noted that both optimal designs meet the geometrical-constraints imposed on the design optimization problem.

Finally, the contour fields of intermittency function are plotted in Fig. (10) for the original and the optimal designs obtained using the "drag minimized" and "transition delayed" approaches. Compared to the NACA 0012 results presented earlier, the boundary layer for this case is much thinner due to the higher

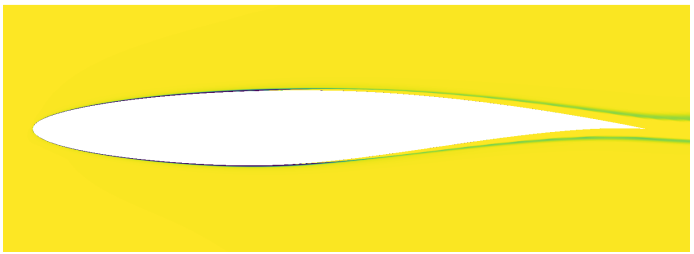

(a) Original

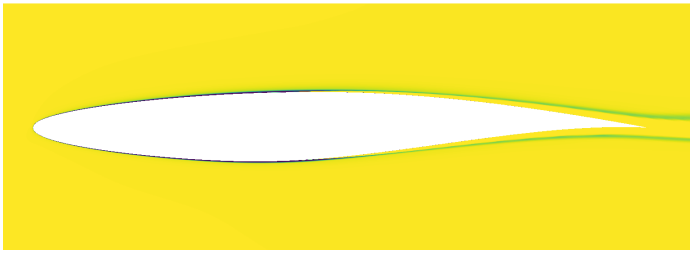

(b) Drag Minimized

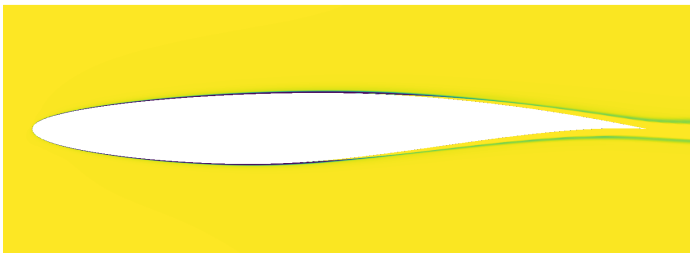

(c) Transition Delayed

Figure 10. Contours of intermittency (SA-AFT2019 model) for the original and the optimal designs of the RAE 2822 airfoil at Mach 0.7, Re = 8 million, and FSTI of 0.15% (target lift $C_L^* = 0.4$). Contour range is from 0 (purple, fully laminar) to 1 (yellow, fully turbulent)

Reynolds number for the RAE 2822 airfoil case. Additionally, it can be easily noticed that the purple region, corresponding to the laminar flow, is expanded for both NLF designs. However, the laminar flow regime on the top side of the optimal airfoil obtained using the proposed approach is significantly expanded compared to the original design. This has resulted in a laminar flow region that covers almost 60% of the airfoil on the suction side, thus significantly reducing the friction drag.

IV. Conclusion

A new technique for aerodynamic shape optimization is featured in this work that aims at attaining natural laminar flow (NLF) designs. The proposed technique focuses on directly delaying the laminar-to-turbulent transition onset on both sides of an airfoil with the goal of expanding the laminar flow regime and reducing the total drag count. A Reynolds-Averaged Navier-Stokes (RANS) solver coupled with the one-equation Spalart-Allmaras (SA) turbulence model and the Amplification Factor Transport (AFT) transition model is utilized for laminar-to-turbulent transition prediction. The AFT model is based on the linear stability method and solves two additional equations for the approximate envelope amplification factor and

the intermittency function. The AFT2019 version used in this work has been recently modified by the authors to achieve a "smooth" and fully-differentiable version that can be used in conjunction with an adjoint-based design optimization framework. The turbulence index profiles on both sides of the airfoil are fed into a non-linear least-squares minimization problem that utilizes a sigmoid fit for an extremely accurate and "differentiable" prediction of the transition onset location. Unlike the conventional approach for NLF design where the friction or total drag coefficients are simply minimized, a new technique is proposed in the present work that utilizes the onset locations for a direct transition delay. The proposed technique is used for the NLF design of a symmetric NACA 0012 and a super critical RAE 2822 airfoil at moderate lift constraints. It is shown that by delaying the transition onset on both the pressure and suction sides, the natural laminar flow region around the airfoil can be greatly expanded, thus resulting in a reduced total drag count. Comparing the conventional and the newly proposed technique, a more pronounced reduction in the friction and total drag counts has been achieved using the direct transition delay approach. Additionally, for the test cases studied in this work, the newly developed technique results in a much more consistent delay of laminar-to-turbulent transition onset location compared to the conventional approach that simply focuses on drag minimization for NLF design.

V. Acknowledgments

This material is based upon work supported by the National Science Foundation under grant No: CBET-1803760. The authors greatly appreciate the support provided.

References

[1]Coder, J. G. and Maughmer, M. D., "A CFD-compatible transition model using an amplification factor transport equation," AIAA Paper 2013-0253, 2013.

[2]Krishnan, K., Bertram, O., and Seibel, O., "Review of hybrid laminar flow control systems," *Progress in Aerospace Sciences*, Vol. 93, 2017, pp. 24–52.

[3]Kalarikovilagam Srinivasan, G. and Bertram, O., "Preliminary design and system considerations for an active hybrid laminar flow control system," *Aerospace*, Vol. 6, No. 10, 2019, pp. 109.

[4]Schrauf, G., Wood, N., and Gölling, B., "Key aerodynamic technologies for aircraft performance improvement," *5th Community Aeronautics Days*, 2006, pp. 19–21.

[5]Halila, G. L., Martins, J. R., and Fidkowski, K. J., "Adjoint-based aerodynamic shape optimization including transition to turbulence effects," *Aerospace Science and Technology*, Vol. 107, 2020, pp. 106243.

[6]Halila, G. L. O., Bigarella, E. D. V., and Azevedo, J. L. F., "Numerical study on transitional flows using a correlation-based transition model," *Journal of Aircraft*, Vol. 53, No. 4, 2016, pp. 922–941.

[7]Halila, G. L. O., Bigarella, E. D. V., Antunes, A. P., and Azevedo, J. L. F., "An efficient setup for freestream turbulence on transition prediction over aerospace configurations," *Aerospace Science and Technology*, Vol. 81, 2018, pp. 259–271.

[8]Halila, G. L. O., Antunes, A. P., da Silva, R. G., and Azevedo, J. L. F., "Effects of boundary layer transition on the aerodynamic analysis of high-lift systems," *Aerospace Science and Technology*, Vol. 90, 2019, pp. 233–245.

[9]Coder, J. G., "Further development of the amplification factor transport transition model for aerodynamic flows," AIAA Paper 2019-0039, 2019.

[10]Somers, D. M., "Design and experimental results for a natural-laminar-flow airfoil for general aviation applications," *NASA Technical Paper (1861)*, 1981.

[11]Langtry, R. and Menter, F., "Transition modeling for general CFD applications in aeronautics," *AIAA paper*, Vol. 522, No. 2005, 2005, pp. 14.

[12]Langtry, R. B. and Menter, F. R., "Correlation-based transition modeling for unstructured parallelized computational fluid dynamics codes," *AIAA Journal*, Vol. 47, No. 12, 2009, pp. 2894–2906.

[13]Lee, J.-D. and Jameson, A., "Natural-laminar-flow airfoil and wing design by adjoint method and automatic transition prediction," AIAA Paper 2009-0897, 2009.

[14]Hanifi, A., Amoignon, O., Pralits, J. O., and Chevalier, M., "A gradient-based optimization method for natural laminar flow design," *Seventh IUTAM Symposium on Laminar-Turbulent Transition*, Springer, 2010, pp. 3–10.

[15]Campbell, R. L., Campbell, M. L., and Streit, T., "Progress toward efficient laminar flow analysis and design," AIAA Paper 2011-3527, 2011.

[16]Cameron, L., Early, J., and McRoberts, R., "Metamodel Assisted Multi-Objective Global Optimisation of Natural Laminar Flow Aerofoils," AIAA Paper 2011-3001, 2011.

[17]Khayatzadeh, P. and Nadarajah, S. K., "Aerodynamic Shape Optimization via Discrete Viscous Adjoint Equations for the k- ω SST Turbulence and γ-$Re_{\theta t}$ Transition Models," AIAA Paper 2011-1247, 2011.

[18]Khayatzadeh, P. and Nadarajah, S. K., "Aerodynamic shape optimization of natural laminar flow (NLF) airfoils," AIAA Paper 2012-0061, 2012.

[19]Howison, J. and Ekici, K., "Dynamic stall analysis using harmonic balance and correlation-based γ-$Re_{\theta t}$ transition models for wind turbine applications," *Wind Energy*, Vol. 18, No. 12, 2015, pp. 2047–2063.

[20]Arnal, D., Casalis, G., and Houdeville, R., "Practical transition prediction methods: subsonic and transonic flows," *VKI Lectures Series Advances in Laminar-Turbulent Transition Modelling*, 2008.

[21]Medida, S., *Correlation-based Transition Modeling for External Aerodynamic Flows*, Ph.D. thesis, University of Maryland College Park, 2014.

[22]Smith, A. M. O., "Transition, pressure gradient and stability theory," *Douglas Aircraft Co., Report ES 26388*, 1956.

[23]Van Ingen, J., "A suggested semi-empirical method for the calculation of the boundary layer transition region," *Technische Hogeschool Delft, Vliegtuigbouwkunde, Rapport VTH-74*, 1956.

[24]Rashad, R. and Zingg, D. W., "Aerodynamic Shape Optimization for Natural Laminar Flow Using a Discrete-Adjoint Approach," *AIAA Journal*, 2016.

[25]Mayle, R., "The role of laminar-turbulent transition in gas turbine engines," *Journal of Turbomachinery*, Vol. 113, 1991, pp. 509–537.

[26]Abu-Ghannam, B. and Shaw, R., "Natural transition of boundary layers—the effects of turbulence, pressure gradient, and flow history," *Journal of Mechanical Engineering Science*, Vol. 22, No. 5, 1980, pp. 213–228.

[27]Menter, F. R., "Two-equation eddy-viscosity turbulence models for engineering applications," *AIAA Journal*, Vol. 32, No. 8, 1994, pp. 1598–1605.

[28]Medida, S. and Baeder, J. D., "Application of the correlation-based γ-$\mathrm{Re}_{\theta t}$ transition model to the Spalart-Allmaras turbulence model," AIAA Paper 2011-3979, 2011.

[29]Spalart, P. and Allmaras, S., "A one-equation turbulence model for aerodynamic flows," AIAA Paper 1992-439, 1992.

[30]Bas, O., Cakmakcioglu, S. C., and Kaynak, U., "A novel intermittency distribution based transition model for low-Re number airfoils," AIAA Paper 2013-2531, 2013.

[31]Smith, A. and Gamberoni, N., "Transition, pressure gradient and stability theory," *Douglas Aircraft Rept. ES-26388*, 1956.

[32]Van Ingen, J., "A suggested semi-empirical method for the calculation of the boundary layer transition region," *Technische Hogeschool Delft, Vliegtuigbouwkunde, Rapport VTH-74*, 1956.

[33]Coder, J. G., *Development of a CFD-compatible transition model based on linear stability theory*, Ph.D. thesis, The Pennsylvania State University, 2014.

[34]Langtry, R. B. and Menter, F. R., "Correlation-based transition modeling for unstructured parallelized computational fluid dynamics codes," *AIAA journal*, Vol. 47, No. 12, 2009, pp. 2894–2906.

[35]Yang, X.-S., *Nature-inspired optimization algorithms*, Academic Press, 2020.

[36]Djeddi, R., Floyd, C. D., Coder, J. G., and Ekici, K., "Adjoint-Based Uncertainty Quantification and Calibration of RANS-Based Transition Modeling," AIAA Paper 2021-3036, 2021.

[37]Shi, Y., Mader, C. A., He, S., Halila, G. L., and Martins, J. R., "Natural Laminar-Flow Airfoil Optimization Design Using a Discrete Adjoint Approach," *AIAA Journal*, Vol. 58, No. 11, 2020, pp. 4702–4722.

[38]Kaya, H. and Tuncer, İ. H., "Discrete Adjoint-Based Aerodynamic Shape Optimization Framework for Natural Laminar Flows," *AIAA Journal*, 2021, pp. 1–16.

[39]Campbell, R. L. and Lynde, M. N., "Building a practical natural laminar flow design capability," AIAA Paper 2017-3059, 2017.

[40]Cella, U., Quagliarella, D., Donelli, R., and Imperatore, B., "Design and test of the UW-5006 transonic natural-laminar-flow wing," *Journal of aircraft*, Vol. 47, No. 3, 2010, pp. 783–795.

[41]Coder, J. G. and Maughmer, M. D., "Computational fluid dynamics compatible transition modeling using an amplification factor transport equation," *AIAA journal*, Vol. 52, No. 11, 2014, pp. 2506–2512.

[42]Coder, J. G., "Enhancement of the Amplification Factor Transport Transition Modeling Framework," AIAA Paper 2017-1709, 2017.

[43]Coder, J. G., Pulliam, T. H., and Jensen, J. C., "Contributions to HiLiftPW-3 using structured, overset grid methods," AIAA Paper 2018-1039, 2018.

[44]Drela, M., "MISES implementation of modified Abu-Ghannam/Shaw transition criterion (second revision)," *Massachusetts Institute of Technology Dept. of Aeronautics and Astronautics*, 1998.

[45]Mack, L., "Transition and laminar instability. JPL Publication 77-15," *Jet Propulsion Laboratory, California Institute of Technology, Pasadena, California, USA*, 1977.

[46]Allmaras, S. R. and Johnson, F. T., "Modifications and clarifications for the implementation of the Spalart-Allmaras turbulence model," *Seventh international conference on computational fluid dynamics (ICCFD7)*, 2012, pp. 1–11.

[47]Shimoda, M., Azegami, H., and Sakurai, T., "Numerical Solution for Min-Max Shape Optimization Problems: Minimum Design of Maximum Stress and Displacement," *JSME International Journal Series A Solid Mechanics and Material Engineering*, Vol. 41, No. 1, 1998, pp. 1–9.

[48]Poon, N. M. and Martins, J. R., "An adaptive approach to constraint aggregation using adjoint sensitivity analysis," *Structural and Multidisciplinary Optimization*, Vol. 34, No. 1, 2007, pp. 61–73.

[49]Djeddi, R. and Ekici, K., "Aerodynamic Shape Optimization Framework Based on a Novel Fully-Automated Adjoint Differentiation Toolbox," AIAA Paper 2019-3201, 2019.

[50]Djeddi, R. and Ekici, K., "Novel Expression-Template-Based Automatic Differentiation of Fortran Codes for Aerodynamic Optimization," *AIAA Journal*, pp. 1–16.

[51]Djeddi, S., *Towards Adaptive and Grid-Transparent Adjoint-Based Design Optimization Frameworks*, Ph.D. thesis, University of Tennessee, 2018.

[52]Djeddi, R. and Ekici, K., "FDOT: A Fast, Memory-Efficient and Automated Approach for Discrete Adjoint Sensitivity Analysis using the Operator Overloading Technique," *Aerospace Science and Technology*, Vol. 91, 2019, pp. 159–174.

[53]Djeddi, R. and Ekici, K., "Discrete Adjoint Recursive Technique for Aerodynamic Design Optimization," AIAA Paper 2021-3035, 2021.